

Research Article

Open Access



# Wavelength-tunable deep blue emission from pure bromide-based colloidal perovskite nanocrystals

Su Hwan Lee<sup>1,#</sup>, Serim Cho<sup>1,#</sup>, Bongjun Yeom<sup>2</sup>, Young-Hoon Kim<sup>1</sup>

<sup>1</sup>Department of Energy Engineering, Hanyang University, Seoul 04763, Republic of Korea.

<sup>2</sup>Department of Chemical Engineering, Hanyang University, Seoul 04763, Republic of Korea.

#Authors contributed equally.

**Correspondence to:** Prof. Young-Hoon Kim, Department of Energy Engineering, Hanyang University, 222 Wangsimni-ro, Seongdong, Seoul 04763, Republic of Korea. E-mail: younghoonkim@hanyang.ac.kr

**How to cite this article:** Lee, S. H.; Cho, S.; Yeom, B.; Kim, Y. H. Wavelength-tunable deep blue emission from pure bromide-based colloidal perovskite nanocrystals. *Microstructures* 2025, 5, 2025054. <https://dx.doi.org/10.20517/microstructures.2024.93>

**Received:** 29 Sep 2024 **First Decision:** 21 Nov 2024 **Revised:** 26 Dec 2024 **Accepted:** 22 Jan 2025 **Published:** 23 Apr 2025

**Academic Editors:** Sang Hyuk Im, Shiqing Deng **Copy Editor:** Ping Zhang **Production Editor:** Ping Zhang

## Abstract

Metal halide perovskites are promising light emitters due to their tunable and highly pure emission color in visible light. However, achieving deep blue emission remains a major challenge due to low stability and intrinsic defects. Traditional methods for synthesizing blue-emitting colloidal perovskite nanocrystals (PNCs) involve organic ammonium engineering and halide engineering, which often suffer from problems such as ion migration and color instability. In this study, we demonstrate a novel central metal engineering approach that achieves deep blue emission with a wavelength of 435.8 nm from pure bromide-based PNCs at room temperature. To synthesize deep blue-emitting pure-bromide-based PNCs, we incorporate manganese bromide ( $\text{MnBr}_2$ ) to the formamidinium-guanidinium lead bromide ( $\text{FA}_{0.9}\text{GA}_{0.1}\text{PbBr}_3$ ) PNCs.  $\text{Mn}^{2+}$  suppresses the growth of  $\text{FA}_{0.9}\text{GA}_{0.1}\text{PbBr}_3$  crystals during the synthesis, resulting in decreases in both particle size and dimensionality and deep blue emission by the quantum confinement effect. The emission wavelength of pure-bromide-based PNCs is controlled by varying the amount of  $\text{MnBr}_2$ . This study provides an effective and simple method for achieving deep blue emission from pure bromide-based PNCs, offering significant advantages for display technologies such as light-emitting diodes.

**Keywords:** Deep blue emission, perovskite nanocrystal, central metal engineering, quantum confinement effect, ligand-assisted reprecipitation



© The Author(s) 2025. **Open Access** This article is licensed under a Creative Commons Attribution 4.0 International License (<https://creativecommons.org/licenses/by/4.0/>), which permits unrestricted use, sharing, adaptation, distribution and reproduction in any medium or format, for any purpose, even commercially, as long as you give appropriate credit to the original author(s) and the source, provide a link to the Creative Commons license, and indicate if changes were made.



## INTRODUCTION

Metal halide perovskites (MHPs) consist of three ions in an  $ABX_3$  structure, where A is an organic ammonium {e.g., methylammonium (MA;  $CH_3NH_3^+$ ), formamidinium [FA;  $CH(NH_2)_2^+$ ]} or an alkali-metal cation (e.g.,  $Cs^+$ ), B is a transition-metal cation (e.g.,  $Pb^{2+}$ ,  $Au^{2+}$ ,  $Sn^{2+}$ ,  $Mn^{2+}$ ), and X is a halide anion (I, Br, Cl). Among many types of MHPs, colloidal perovskite nanocrystals (PNCs) have been considered potential light emitters because PNCs emit light with high color purity [full width at half maximum (FWHM)  $\sim 20$  nm] and also have controllable wavelengths (400 nm to 800 nm)<sup>[1–8]</sup>. Recently, green-emitting and red-emitting PNCs, which exhibited high photoluminescence quantum yield (PLQY), have been reported along with highly efficient perovskite light-emitting diodes (PeLEDs)<sup>[9–14]</sup>. However, the development of blue emission with high PLQY remains challenging because of its low stability and intrinsic defect<sup>[15–19]</sup>.

Conventionally, X-site anion engineering has been attempted to synthesize blue-emitting PNCs<sup>[19]</sup>. While the conduction band is formed by antibonding mixing of the  $6p^6$  orbitals of lead metal and the  $np^6$  orbitals of halide ( $n = 3, 4$ , and  $5$  for Cl, Br, and I, respectively), the valence band is formed primarily by mixing of the  $np^6$  orbitals of halide and the  $6s^2$  orbitals of lead metal<sup>[20]</sup>. The energy of the  $np^6$  orbitals of halide decreases as the halide moves from I ( $5p^6$ ) to Br ( $4p^6$ ) to Cl ( $3p^6$ ), shifting the valence band maximum to higher positive potentials. Thus, a systematic change in the halide composition of  $CsPbX_3$  PNCs from  $CsPbI_3$  and  $CsPbBr_3$  to  $CsPbCl_3$  results in an increase in the bandgap and blue-shift in the emitting wavelength. For example, Protesescu *et al.* demonstrated blue light with tunable wavelengths from 410 nm to 460 nm using Cl-based mixed halides in inorganic lead halide perovskites ( $CsPbX_3$ )<sup>[19]</sup>. However, in mixed-halide PNCs developed through X-site engineering, an applied electric field to the PNC films in PeLEDs can induce ion migration and the change of luminescence color because halide ions have low activation energy for ion migration<sup>[3]</sup>. Furthermore, addition of chloride induces deep-level trap states in the bandgap, which reduces the device efficiency<sup>[21]</sup>. Therefore, it is important to achieve blue emission from pure halide PNCs.

A-site cation engineering has been tried to achieve blue emission from pure bromide PNCs<sup>[21]</sup>. Large-sized A-site cations induce smaller-sized PNCs by suppressing their growth<sup>[22]</sup> or lead to low-dimensional PNCs by restricting their expansion in the orthogonal direction<sup>[23–25]</sup>. In these PNCs, an increased bandgap and blue-shifted photoluminescence (PL) are observed due to quantum-confinement effect<sup>[25]</sup> or dielectric confinement effect<sup>[26]</sup> although A-site cations do not directly participate in the band edge<sup>[21]</sup>. Despite the successful blue emission from pure-halide PNCs through A-site engineering, A-site engineered blue-emitting PNCs can suffer from low electrical mobility in thin films because large-sized A-site cations are insulating and impede charge transport. To overcome the limitations of A-site and X-site engineering for the synthesis of blue-emitting PNCs and PeLEDs, B-site engineering can be an alternative method to achieve stable and wavelength-tunable blue emission from pure-halide PNCs.

Recently, B-site engineering has been attempted to achieve blue emission from pure halide PNCs. Wang *et al.* reported that incorporating  $Zn^{2+}$  into the precursor solution retards the growth of perovskite crystals, leading to FA lead bromide ( $FAPbBr_3$ ) PNCs with smaller size and thus achieving blue emission<sup>[27]</sup>. The wavelength of emitted light can be tuned by controlling the amount of  $Zn^{2+}$ ; however, the wavelength is limited to above 486 nm, resulting in a sky-blue color. To demonstrate high color purity displays and cover the wide range in International Commission on Illumination (CIE) chromaticity coordinate, new B-site engineering methods that enable deep blue emission (Royal blue color) with a wavelength below 450 nm from pure-halide PNCs should be developed.

Here, we report a new B-site engineering strategy that enables deep blue emission with a controllable wavelength from Br-based PNCs. We employ manganese cation ( $\text{Mn}^{2+}$ ) during the synthesis of PNCs.  $\text{Mn}^{2+}$  inhibits crystal growth, resulting in the formation of smaller particles. Additionally, as the Mn concentration increases,  $\text{Mn}^{2+}$  ions inhibit the growth of the  $[\text{PbBr}_6]^{4-}$  octahedra along the orthogonal direction, leading to the formation of two-dimensional (2D) structures and allowing the surface amine-based ligand to diffuse between 2D octahedral layers [Figure 1A]. The reduction in both particle size and dimensionality induces a significant blue shift in the emission spectrum, down to 435.8 nm, from pure-Br-based PNCs. The wavelength can be controlled by varying the  $\text{Mn}^{2+}$  concentration. These results demonstrate the potential of B-site engineering as a promising approach for developing deep blue emitters in display technologies.

## METHODS

### Synthesis

All  $\text{FA}_{0.9}\text{GA}_{0.1}\text{Pb}_{1-x}\text{Mn}_x\text{Br}_3$  PNCs were synthesized in the air at room temperature. Precursor solutions were prepared by dissolving FABr (Dyesol), guanidinium bromide (GABr) (Dyesol),  $\text{PbBr}_2$  (TCI, 99.999%), and  $\text{MnBr}_2$  (Aldrich 98%), with the  $\text{PbBr}_2\text{:MnBr}_2$  input ratio changing from 1:0 ( $x = 0$ ) to 0.1:0.9 ( $x = 0.9$ ) while maintaining the molarity of  $\text{MnBr}_2\text{:PbBr}_2$  at 0.1 mmol and the molarity of FABr:GABr at 0.2 mmol each in 0.5 mL of anhydrous N,N-dimethylformamide (DMF) (Aldrich, 99.8%); 0.15 mL of precursor solution was then dropped into a crystallization-inducing solution comprising 5 mL of toluene (Aldrich, 99.8%), 2 mL of 1-butanol (SAMCHUN, 99.5%), 0.3 mL of oleic acid (Aldrich, 90%) and 20.4  $\mu\text{L}$  of n-decylamine (Aldrich, 99.0%), which was mixed for 10 min under vigorous stirring. The resulting colloidal PNCs were washed by sequential centrifugation and then collected in 2 mL of toluene (Aldrich, 99.8%).

### Characterization

X-ray diffraction (XRD) patterns were measured using a Rigaku Ultima with target Cu K $\alpha$  radiation ( $\lambda = 1.54 \text{ \AA}$ ) at 40 kV and 40 mA. Electronic absorption spectra were measured using a JASCO V-730 ultraviolet-visible (UV-Vis) spectrophotometer. The PL and PLQYs of PNCs were measured using a spectrofluorometer (FP-8550, Jasco Inc., Japan). PLQYs were measured using an absolute PLQY spectrometer with an integrating sphere (ILF-135) [Supplementary Scheme 1]. PL spectra time-correlated single photon counting (TCSPC) was measured using a PicoQuant FluoTime 300 EasyTau with a 405 nm pulsed laser diode. To measure the high-resolution transmission electron microscopy (HR-TEM) images of the PNCs, 0.05 mL of PNC solutions were dropped onto a copper grid and measured using a JEOL-JEM 2100F with an acceleration voltage of 200 kV.

## RESULTS

### Synthesis of wavelength-controllable blue-emitting $\text{FA}_{0.9}\text{GA}_{0.1}\text{Pb}_{1-x}\text{Mn}_x\text{Br}_3$ PNCs

We synthesized FA-GA lead bromide ( $\text{FA}_{0.9}\text{GA}_{0.1}\text{PbBr}_3$ ) PNCs and  $\text{FA}_{0.9}\text{GA}_{0.1}\text{Pb}_{1-x}\text{Mn}_x\text{Br}_3$  PNCs by the ligand-assisted reprecipitation (LARP) method. Here, we selected  $\text{FA}_{0.9}\text{GA}_{0.1}\text{PbBr}_3$  PNCs because we reported that  $\text{FA}_{0.9}\text{GA}_{0.1}\text{PbBr}_3$  PNCs can achieve extremely high PLQY ( $> 90\%$ ) and high electroluminescence efficiency [external quantum efficiency (EQE)  $> 23.4\%$ ] in PeLEDs in our previous works<sup>[9–10]</sup>. To synthesize the PNCs, we dissolved all the precursors in the DMF solution with different Mn input molar ratios ( $x = 0, 0.1, 0.2, 0.4, 0.6, 0.8$ , and  $0.9$ ) and then injected the solutions into a toluene dispersion containing the ligands. After crystallization, we changed the solvent to toluene by sequential centrifugation (Figure 1B, see Experimental for more information)

As  $x$  increases from 0 to 0.9, PL spectra of  $\text{FA}_{0.9}\text{GA}_{0.1}\text{Pb}_{1-x}\text{Mn}_x\text{Br}_3$  PNCs gradually blue-shift from 528.9 nm to 435.8 nm [Figure 1C]. The appearance of new peaks at the PL spectrum at  $\sim 410 \text{ nm}$  and  $\sim 440 \text{ nm}$  is attributed to dimensionality reduction. This will be discussed in more detail later in Section 3.3. The PL wavelength of 435.8 nm is highly blue-shifted, representing the deep blue (Royal blue) emission

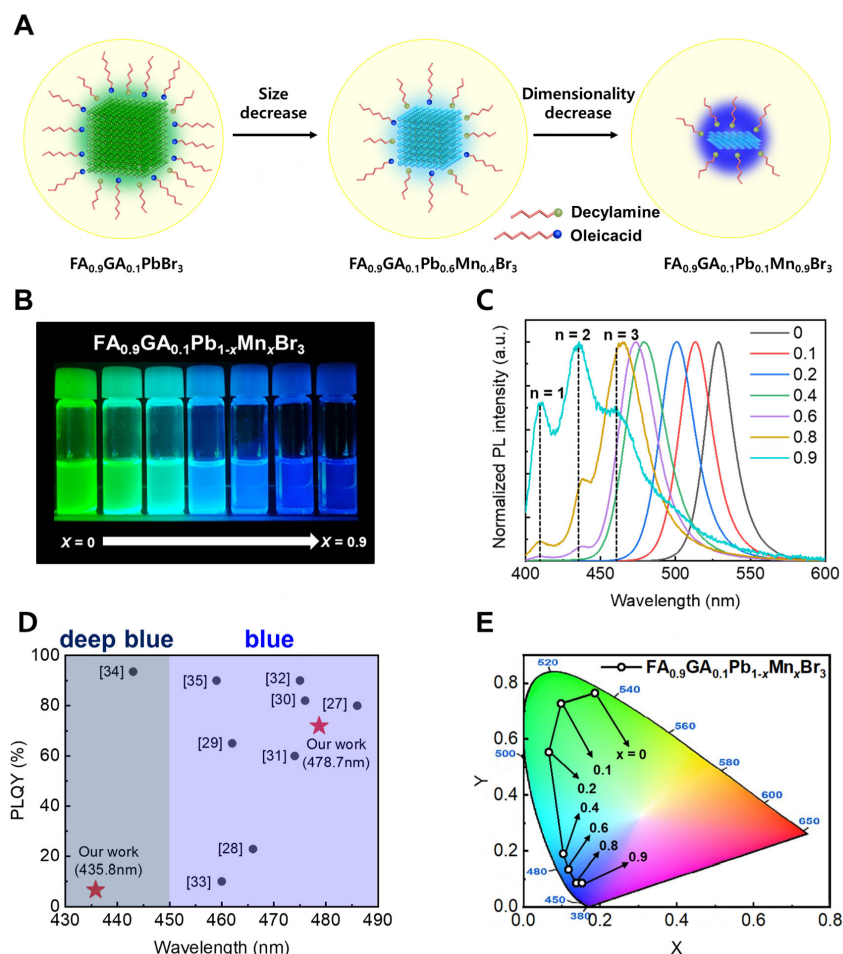


**Figure 1.** (A) A schematic illustration of blue-emitting  $\text{FA}_{0.9}\text{GA}_{0.1}\text{Pb}_{1-x}\text{Mn}_x\text{Br}_3$  PNCs ( $x$  = input ratio) with increasing  $\text{Mn}^{2+}$  concentration; (B) Photograph and (C) measured PL spectra of colloidal  $\text{FA}_{0.9}\text{GA}_{0.1}\text{Pb}_{1-x}\text{Mn}_x\text{Br}_3$  PNC solutions under a UV lamp (excitation wavelength  $\lambda_{\text{ex}}$  = 365 nm); (D) Photoluminescence quantum yield (PLQY) and emission wavelength of  $\text{FA}_{0.9}\text{GA}_{0.1}\text{Pb}_{1-x}\text{Mn}_x\text{Br}_3$  PNCs ( $x$  = 0.4 and 0.9) and previously reported blue-emitting pure bromide-based PNCs [28–35]; (E) CIE coordinates of  $\text{FA}_{0.9}\text{GA}_{0.1}\text{Pb}_{1-x}\text{Mn}_x\text{Br}_3$  PNCs with different  $x$  (black dot points) plotted on CIE chromaticity coordinates. PNCs: Perovskite nanocrystals; PL: photoluminescence; CIE: international commission on illumination.

characteristic of pure bromide-based PNCs [Supplementary Table 1]. We also confirmed the stability and reproducibility of the deep-blue-emitting  $\text{FA}_{0.9}\text{GA}_{0.1}\text{Pb}_{0.1}\text{Mn}_{0.9}\text{Br}_3$  PNCs [Supplementary Figures 1 and 2]. Figure 1D shows the PL performance of  $\text{FA}_{0.9}\text{GA}_{0.1}\text{Pb}_{1-x}\text{Mn}_x\text{Br}_3$  PNCs compared with previously reported literature [Supplementary Table 2].  $\text{FA}_{0.9}\text{GA}_{0.1}\text{Pb}_{1-x}\text{Mn}_x\text{Br}_3$  PNCs cover a wide range in the CIE diagram from pure green light to deep blue light [Figure 1E].

### Size distribution and emission mechanism of $\text{FA}_{0.9}\text{GA}_{0.1}\text{Pb}_{1-x}\text{Mn}_x\text{Br}_3$ PNCs

Next, we investigate the mechanism that incorporation of Mn induces a huge blue-shift in PL from  $\text{FA}_{0.9}\text{GA}_{0.1}\text{Pb}_{1-x}\text{Mn}_x\text{Br}_3$  PNCs. Firstly, we measured HR-TEM images of  $\text{FA}_{0.9}\text{GA}_{0.1}\text{Pb}_{1-x}\text{Mn}_x\text{Br}_3$  PNCs [Figure 2A–C and Supplementary Figure 3]. The  $\text{FA}_{0.9}\text{GA}_{0.1}\text{PbBr}_3$  PNC lattice spacing was measured at approximately 2.95 Å. As  $x$  increased,  $\text{FA}_{0.9}\text{GA}_{0.1}\text{Pb}_{1-x}\text{Mn}_x\text{Br}_3$  PNCs exhibited gradually decreasing average sizes ( $\approx 11.9$  nm for  $x = 0$ ,  $\approx 6.74$  nm for  $x = 0.4$ , and  $\approx 5.79$  nm for  $x = 0.6$ ) [Figure 2D–F]. These TEM images indicate that blue emission can be achieved by reducing the size of  $\text{FA}_{0.9}\text{GA}_{0.1}\text{Pb}_{1-x}\text{Mn}_x\text{Br}_3$  PNCs in the strong quantum confinement regime through appropriate adjustment of the  $\text{Mn}^{2+}$  and  $\text{Pb}^{2+}$  ratio in the perovskite precursor solution.

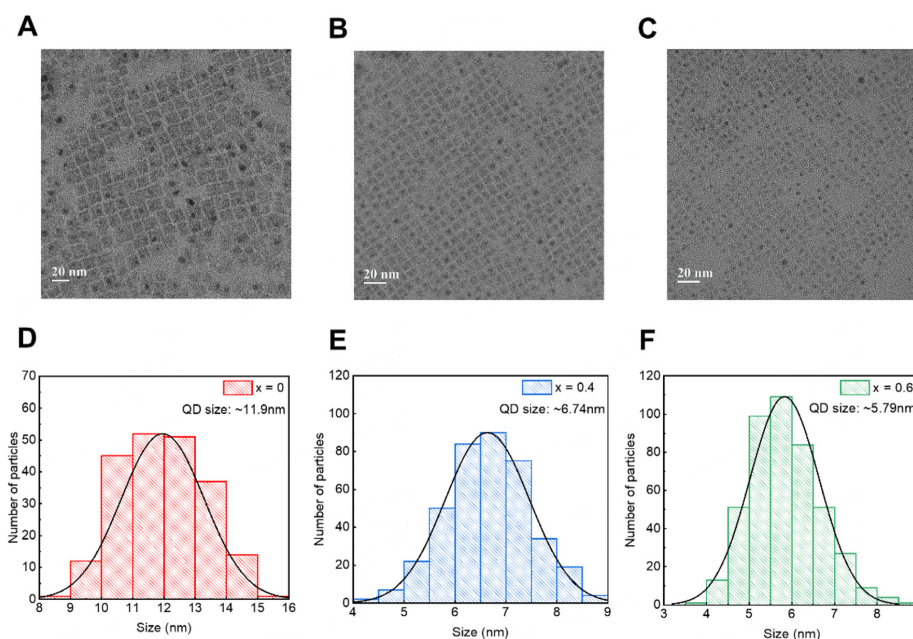


**Figure 2.** HR-TEM images of  $\text{FA}_{0.9}\text{GA}_{0.1}\text{Pb}_{1-x}\text{Mn}_x\text{Br}_3$  PNCs at (A)  $x = 0$ , (B)  $x = 0.4$ , and (C)  $x = 0.6$ ; The size distribution histograms of  $\text{FA}_{0.9}\text{GA}_{0.1}\text{Pb}_{1-x}\text{Mn}_x\text{Br}_3$  PNCs at (D)  $x = 0$ , (E)  $x = 0.4$ , and (F)  $x = 0.6$ . PNCs: Perovskite nanocrystals; HR-TEM: high-resolution transmission electron microscopy.

Conventionally, Mn doping introduces a d-state energy level of the  $\text{Mn}^{2+}$  ions to the bandgap of perovskites, inducing a transition for exciton-to-dopant energy transfer and resulting in orange-red emission from PNCs<sup>[36,37]</sup>. We also observed that  $\text{Mn}^{2+}$  ions produce orange emission with a PL peak at around 600 nm from  $\text{Mn}^{2+}$  doped  $\text{CsPbCl}_3$  PNCs [Supplementary Figure 4]. Liu *et al.* suggest that isovalent ions with similar bond energy can be doped into the lattices while those with different bond energy cannot be<sup>[38]</sup>. For example, the bond dissociation energy of Mn-Cl (338 kJ/mol) is similar to that of Pb-Cl (301 kJ/mol) and therefore  $\text{Mn}^{2+}$  is well-doped in the  $\text{CsPbCl}_3$  host. Moreover, the large bandgap ( $\sim 3.1$  eV) of the  $\text{CsPbCl}_3$  PNCs facilitates energy transfer from host energy level to the energy level of  $\text{Mn}^{2+}$ , resulting in an orange light emission from d-state energy level of  $\text{Mn}^{2+}$ .

In contrast, in Br-based PNCs, Liu *et al.* reported that the bond dissociation energy of the Mn-Br bond (314 kJ/mol) is much stronger than that of the Pb-Br bond (249 kJ/mol), leading to the formation of extended  $\text{MnBr}_2$  domains within  $\text{PbBr}_2$  lattices rather than doping of  $\text{Mn}^{2+}$  within the perovskite lattice<sup>[38]</sup>. Furthermore,  $\text{FA}_{0.9}\text{GA}_{0.1}\text{PbBr}_3$  PNCs have a smaller bandgap of  $\sim 2.31$  eV, with a conduction band minimum (CBM) close to the d-state energy level of  $\text{Mn}^{2+}$ , preventing energy transfer to  $\text{Mn}^{2+}$  and light emission from the d-state energy level of  $\text{Mn}^{2+}$  [Supplementary Figures 5 and 6]<sup>[36,39]</sup>. Hou *et al.* also reported that when  $\text{Mn}^{2+}$  is incorporated into bromide-chloride mixed halide ( $\text{CsMn}_y\text{Pb}_{1-y}\text{Br}_x\text{Cl}_{3-x}$ ) PNCs, orange light is not emitted while blue light is maintained due to the dominance of Br over Cl<sup>[40]</sup>. Therefore, we hypothesize that incorporation of Mn-based precursors during the growth of  $\text{FA}_{0.9}\text{GA}_{0.1}\text{PbBr}_3$  PNCs does not induce  $\text{Mn}^{2+}$ -doped  $\text{FA}_{0.9}\text{GA}_{0.1}\text{PbBr}_3$  PNCs; rather, it forms smaller or low-dimensional  $\text{FA}_{0.9}\text{GA}_{0.1}\text{PbBr}_3$  crystals. In this case,  $\text{Mn}^{2+}$ , which were not doped into  $\text{FA}_{0.9}\text{GA}_{0.1}\text{PbBr}_3$  crystals, suppress the growth of the PNCs, reduce the PNC size and result in blue-shifted PL.

### Structural and optical properties of $\text{FA}_{0.9}\text{GA}_{0.1}\text{Pb}_{1-x}\text{Mn}_x\text{Br}_3$ PNCs

To investigate the effects of Mn doping on the photophysical properties, we measured the time-resolved PL (TRPL) of  $\text{FA}_{0.9}\text{GA}_{0.1}\text{Pb}_{1-x}\text{Mn}_x\text{Br}_3$  PNCs. At  $x = 0$ ,  $\text{FA}_{0.9}\text{GA}_{0.1}\text{PbBr}_3$  PNCs showed a PL lifetime of 58.43 ns



[Figure 3A]. As  $x$  increases to 0.4, the PL lifetime decreases to 23.17 ns because smaller PNCs cause a reduction in PL lifetime<sup>[41]</sup>. This phenomenon can be attributed to enhanced spatial confinement of charge carriers and the boost of their radiative recombination<sup>[42]</sup>.  $\text{FA}_{0.9}\text{GA}_{0.1}\text{Pb}_{1-x}\text{Mn}_x\text{Br}_3$  PNCs also showed a blue-shifted absorption spectrum, indicating that Mn doping decreases the PNC size [Figure 3B].

Next, we measured the PLQY of  $\text{FA}_{0.9}\text{GA}_{0.1}\text{Pb}_{1-x}\text{Mn}_x\text{Br}_3$  PNCs with different  $x$  values (0, 0.1, 0.2, 0.4, 0.6, 0.8, and 0.9) [Figure 3C]. As  $x$  increases to 0.4, PLQY slightly decreases from 87.46% to 71.90% but remains relatively high. We attribute this decrease in PLQY to the increased surface defects due to a higher surface-to-volume ratio and reduced PNC size<sup>[42]</sup>. When  $x$  increases  $> 0.4$ ,  $\text{FA}_{0.9}\text{GA}_{0.1}\text{Pb}_{1-x}\text{Mn}_x\text{Br}_3$  PNCs showed a significant drop in PLQY (43.94% for  $x = 0.6$ , 19.03% for  $x = 0.8$ , and 6.64% for  $x = 0.9$ ). The rapid reduction in PLQY is likely attributed to the increased  $z$ -axis defects, which arise from the decreased dimensionality along this axis and introduce non-radiative recombination pathways<sup>[25]</sup>. A more detailed discussion on the impact of dimensionality reduction is provided in a later section. The trend of the sudden decrease in PLQY for  $x > 0.4$  is different from that for  $x < 0.4$ .

To investigate the reason for a significant decrease in PLQY at  $x > 0.4$ , we measured the XRD peaks of  $\text{FA}_{0.9}\text{GA}_{0.1}\text{Pb}_{1-x}\text{Mn}_x\text{Br}_3$  PNCs ( $x = 0, 0.1, 0.2, 0.4, 0.6, 0.8$ , and  $0.9$ ) [Figure 3D and Supplementary Figure 7]. At  $x = 0.1$  and  $0.2$ ,  $\text{FA}_{0.9}\text{GA}_{0.1}\text{Pb}_{1-x}\text{Mn}_x\text{Br}_3$  PNCs showed XRD peaks at  $12.5^\circ$ ,  $15^\circ$ ,  $25^\circ$  and  $30^\circ$ , which correspond to (001), (110), (111), and (220) crystal planes, respectively, similar to those of  $\text{FA}_{0.9}\text{GA}_{0.1}\text{PbBr}_3$  PNCs<sup>[10,43]</sup>. These results indicate that  $\text{FA}_{0.9}\text{GA}_{0.1}\text{Pb}_{1-x}\text{Mn}_x\text{Br}_3$  PNCs maintain the cubic crystal structure and  $\text{Mn}^{2+}$  ions are not incorporated into the  $\text{FA}_{0.9}\text{GA}_{0.1}\text{PbBr}_3$  lattices for  $x < 0.4$ .

At  $x \geq 0.4$ ,  $\text{FA}_{0.9}\text{GA}_{0.1}\text{Pb}_{1-x}\text{Mn}_x\text{Br}_3$  PNCs exhibited sharp XRD patterns with  $\approx 3.6$  two theta degree spacing ( $10.7^\circ$ ,  $14.3^\circ$ ,  $17.9^\circ$ ,  $21.5^\circ$ ,  $25.1^\circ$  and  $28.7^\circ$ , corresponding to the (0 0  $l$ ) planes), which are notably different from those of  $\text{FA}_{0.9}\text{GA}_{0.1}\text{Pb}_{1-x}\text{Mn}_x\text{Br}_3$  PNCs for  $x < 0.4$ . (0 0  $l$ ) indices with sharp peaks in the PNCs indicate that crystals with low dimensionality are synthesized when a large amount of  $\text{Mn}^{2+}$  is incorporated during the synthesis. However, at  $x = 1$  without Pb,  $\text{FA}_{0.9}\text{GA}_{0.1}\text{MnBr}_3$  PNCs did not show a sharp peak in XRD. The absence of XRD peaks and absorption/PL spectrum indicate that  $\text{FA}_{0.9}\text{GA}_{0.1}\text{MnBr}_3$  PNCs were not well synthesized by our LARP method. According to Bragg's law, the interlayer spacing  $d$  of low-dimensional PNCs for  $x \geq 0.4$  was calculated to be  $2.45 \text{ nm}$ <sup>[44]</sup>. Using the relationship between  $d$  and alkyl chain length  $n$  of the organic ligand between Br-based low-dimensional octahedral layers [ $d (\text{\AA}) = 8.06 + 1.59 \times n$ ]<sup>[45]</sup>, the value of  $n$  is calculated to be  $\approx 10$ . This indicates that among organic ligands [decylamine ( $\text{C}_{10}\text{H}_{21}\text{NH}_2$ ), oleic acid ( $\text{C}_{18}\text{H}_{33}\text{O}_2\text{H}$ )] added into the precursor solution, decylamine is located between the 2D PNC layers, suppressing the growth of crystals along the out of plane direction and resulting in low-dimensional PNCs.

Zhang *et al.* suggested that preferential binding of amine ligands to the certain facet of the perovskite crystals results in low-dimensional  $\text{CsPbX}_3$  nanowires<sup>[46]</sup>. Pan *et al.* revealed that ammonium ions effectively tune the growth of anisotropic perovskite structures, and shorter chain ammonium ions diffuse faster than longer chain ones, resulting in thinner platelets<sup>[47]</sup>. Therefore, we attribute the insertion of decylamine between the 2D PNC layers rather than oleic acid to the fact that decylamine has shorter alkyl length than longer oleic acid, amine-group has higher mobility than carboxylic acid, and thus decylamine diffuses between the 2D layers more easily<sup>[47,48]</sup>. In addition to the change in XRD patterns, new peaks in the PL spectrum at  $\sim 410 \text{ nm}$  (Peak 3) and  $\sim 440 \text{ nm}$  (Peak 2) started to appear from  $x = 0.4$  [Figure 1C and Supplementary Figure 8]. The absorption spectrum at a short wavelength corroborates that  $\text{FA}_{0.9}\text{GA}_{0.1}\text{Pb}_{1-x}\text{Mn}_x\text{Br}_3$  PNCs with low dimensionality ( $n = 1$  and  $2$ ) are formed as  $x$  increases ( $x > 0.4$ ) [Figure 1C and Supplementary Figure 9].

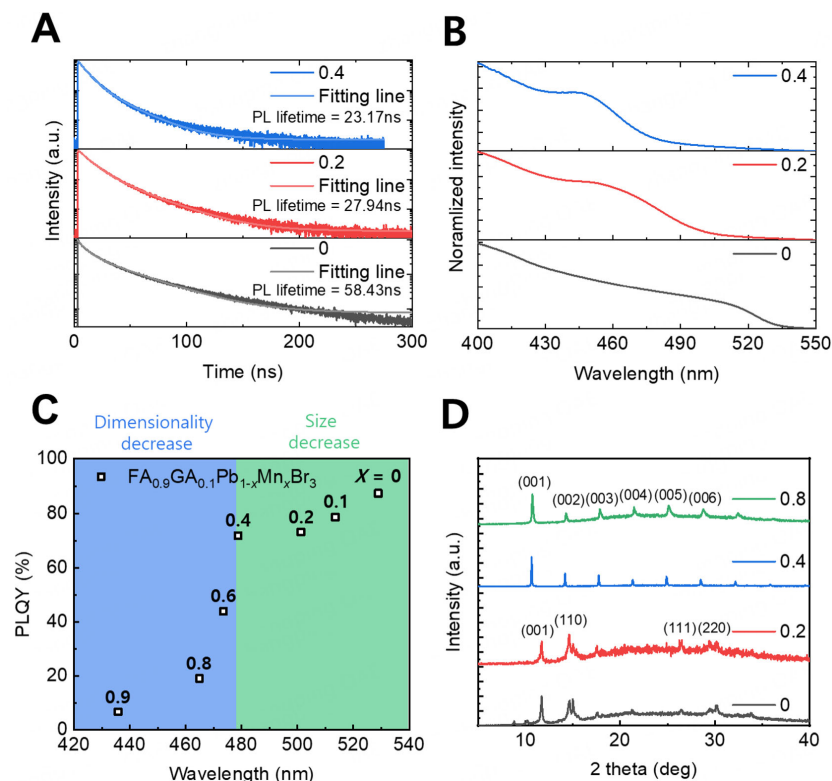


**Figure 3.** (A) PL decay profiles and (B) absorption spectra of  $\text{FA}_{0.9}\text{GA}_{0.1}\text{Pb}_{1-x}\text{Mn}_x\text{Br}_3$  PNCs ( $x = 0, 0.2, 0.4$ ); (C) PLQY and emission wavelength of  $\text{FA}_{0.9}\text{GA}_{0.1}\text{Pb}_{1-x}\text{Mn}_x\text{Br}_3$  PNCs at  $0 \leq x \leq 0.9$ . (D) XRD patterns of series of the  $\text{FA}_{0.9}\text{GA}_{0.1}\text{Pb}_{1-x}\text{Mn}_x\text{Br}_3$  PNCs at  $0 \leq x \leq 0.8$ . PL: Photoluminescence; PNCs: perovskite nanocrystals; PLQY: photoluminescence quantum yield; XRD: X-ray diffraction.

### Mechanism of size reduction and dimensionality control

Next, we consider mechanisms by which the incorporation of  $\text{Mn}^{2+}$  plays a critical role in controlling the size and dimensionality of PNCs [Figure 4]. First,  $\text{Mn}^{2+}$  cannot be doped into the  $\text{FA}_{0.9}\text{GA}_{0.1}\text{PbBr}_3$  PNCs because the Mn-Br has higher bond energy than the Pb-Br bond (249 kJ/mol).  $\text{Mn}^{2+}$  ions, which were not doped into  $\text{FA}_{0.9}\text{GA}_{0.1}\text{PbBr}_3$  crystals, coordinate more strongly with *n*-decylammonium bromide ligands or oleate ligands than do  $\text{Pb}^{2+}$  ions, following the principle of the soft acid-base theory. At  $x < 0.4$ , this stronger coordination retards the diffusion of  $\text{Br}^-$  ions from precursor solutions to crystals and suppresses the growth of  $\text{FA}_{0.9}\text{GA}_{0.1}\text{PbBr}_3$  crystals, resulting in small-sized  $\text{FA}_{0.9}\text{GA}_{0.1}\text{PbBr}_3$  PNCs. At  $x \geq 0.4$ , excess  $\text{Mn}^{2+}$ -species [ $\text{Mn}^{2+}$ -oleate ( $\text{C}_{17}\text{H}_{33}\text{COO}^-$ ) and  $\text{Mn}^{2+}$ -*n*-decylammonium bromide ( $\text{C}_{10}\text{H}_{21}\text{NH}_3^+\text{Br}^-$ )] greatly suppress the growth of  $\text{FA}_{0.9}\text{GA}_{0.1}\text{PbBr}_3$  crystals, allowing decylamine to diffuse onto the top surface of low-dimensional  $\text{FA}_{0.9}\text{GA}_{0.1}\text{PbBr}_3$  crystal layers. As a result,  $\text{FA}_{0.9}\text{GA}_{0.1}\text{PbBr}_3$  nanoplatelets with low dimensionality ( $n = 1, 2, 3$ ) are formed, emitting a highly deep blue emission with a wavelength of 435.8 nm at  $x = 0.8$  [Supplementary Table 2].

### CONCLUSIONS

In summary, we demonstrated highly deep blue emission with a wavelength of 435.8 nm from pure-Br-based PNCs. To achieve this, we utilized  $\text{Mn}^{2+}$  as a dopant of  $\text{FA}_{0.9}\text{GA}_{0.1}\text{PbBr}_3$  PNCs.  $\text{Mn}^{2+}$  inhibits crystal growth and results in the formation of smaller particles. At high Mn concentration,  $\text{Mn}^{2+}$  ions also inhibit the growth of the  $[\text{PbBr}_6]^{4-}$  octahedra along the orthogonal direction, allowing the organic ligands to diffuse on the low-dimensional  $[\text{PbBr}_6]^{4-}$  octahedra and resulting in low-dimensional PNCs. These both reduced particle size and dimensionality induce a huge blue shift in pure-Br-based PNCs. The emission wavelength can be controlled from 528.9 nm to 435.8 nm by varying the input Mn concentration. These findings

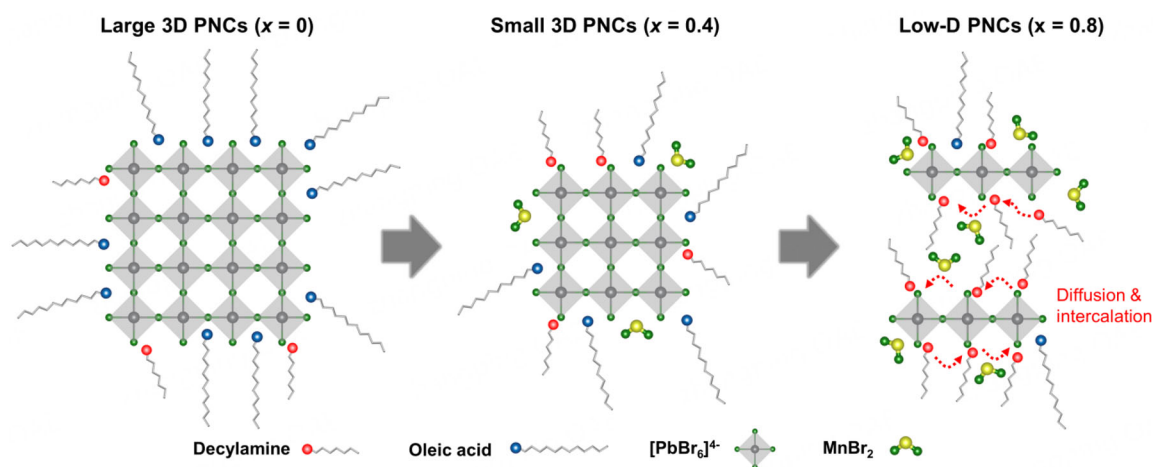


**Figure 4.** A schematic illustration of size and dimensionality reduction of  $\text{FA}_{0.9}\text{GA}_{0.1}\text{Pb}_{1-x}\text{Mn}_x\text{Br}_3$  PNCs with increasing  $\text{Mn}^{2+}$  concentration. PNCs: Perovskite nanocrystals.

highlight the potential of B-site engineering as a viable approach for synthesizing deep blue emitters for display technologies such as light-emitting diodes.

## DECLARATIONS

### Authors' contributions

Data acquisition and analysis: Lee, S. H.; Cho, S.

Design, writing review and editing: Lee, S. H.; Cho, S.; Kim, Y. H.

Supervised the project: Yeom, B.; Kim, Y.H.

### Availability of data and materials

Some results of supporting the study are presented in the [Supplementary Materials](#). Other raw data that support the findings of this study are available from the corresponding author upon reasonable request.

### Financial support and sponsorship

This work was supported by the National Research Foundation of Korea (NRF) (No. RS-2024-00408951). This research was supported by the Digital Research Innovation Institution Program Through the NRF funded by the Ministry of Science and ICT (RS-2023-00283597).

### Conflicts of interest

All authors declared that there are no conflicts of interest.

### Ethical approval and consent to participate

Not applicable.

### Consent for publication

Not applicable.

### Copyright

© The Author(s) 2025.



## REFERENCES

- Schmidt, L. C.; Pertegás, A.; González-Carrero, S.; et al. Nontemplate synthesis of  $\text{CH}_3\text{NH}_3\text{PbBr}_3$  perovskite nanoparticles. *J. Am. Chem. Soc.* **2014**, *136*, 850-3. DOI
- Kim, Y. H.; Cho, H.; Lee, T. W. Metal halide perovskite light emitters. *Proc. Natl. Acad. Sci. U. S. A.* **2016**, *113*, 11694-702. DOI PubMed PMC
- Kim, Y. H.; Kim, J. S.; Lee, T. W. Strategies to improve luminescence efficiency of metal-halide perovskites and light-emitting diodes. *Adv. Mater.* **2019**, *31*, 1804595. DOI PubMed
- Koscher, B. A.; Swabeck, J. K.; Bronstein, N. D.; Alivisatos, A. P. Essentially trap-free  $\text{CsPbBr}_3$  colloidal nanocrystals by postsynthetic thiocyanate surface treatment. *J. Am. Chem. Soc.* **2017**, *139*, 6566-9. DOI
- De, R. J.; Ibáñez, M.; Geiregat, P.; et al. Highly dynamic ligand binding and light absorption coefficient of cesium lead bromide perovskite nanocrystals. *ACS. Nano.* **2016**, *10*, 2071-81. DOI
- Wang, H.; Wang, W.; Tang, A.; et al. High-performance  $\text{CsPb}_{1-x}\text{Sn}_x\text{Br}_3$  perovskite quantum dots for light-emitting diodes. *Angew. Chem. Int. Ed.* **2017**, *129*, 13838-42. DOI
- Chiba, T.; Hayashi, Y.; Ebe, H.; et al. Anion-exchange red perovskite quantum dots with ammonium iodine salts for highly efficient light-emitting devices. *Nature. Photon.* **2018**, *12*, 681-7. DOI
- Song, J.; Fang, T.; Li, J.; et al. Organic-inorganic hybrid passivation enables perovskite QLEDs with an EQE of 16.48%. *Adv. Mater.* **2018**, *30*, e1805409. DOI
- Kim, Y. H.; Park, J.; Kim, S.; et al. Exploiting the full advantages of colloidal perovskite nanocrystals for large-area efficient light-emitting diodes. *Nat. Nanotechnol.* **2022**, *17*, 590-7. DOI
- Kim, Y.; Kim, S.; Kakekhani, A.; et al. Comprehensive defect suppression in perovskite nanocrystals for high-efficiency light-emitting diodes. *Nat. Photonics.* **2021**, *15*, 148-55. DOI
- Kong, L.; Sun, Y.; Zhao, B.; et al. Fabrication of red-emitting perovskite LEDs by stabilizing their octahedral structure. *Nature* **2024**, *631*, 73-9. DOI
- Li, G.; Huang, J.; Zhu, H.; Li, Y.; Tang, J.; Jiang, Y. Surface ligand engineering for near-unity quantum yield inorganic halide perovskite QDs and high-performance QLEDs. *Chem. Mater.* **2018**, *30*, 6099-107. DOI
- Dong, Y.; Wang, Y. K.; Yuan, F.; et al. Bipolar-shell resurfacing for blue LEDs based on strongly confined perovskite quantum dots. *Nat. Nanotechnol.* **2020**, *15*, 668-74. DOI
- Chen, C.; Xuan, T.; Bai, W.; et al. Highly stable  $\text{CsPbI}_3\text{:Sr}^{2+}$  nanocrystals with near-unity quantum yield enabling perovskite light-emitting diodes with an external quantum efficiency of 17.1%. *Nano. Energy.* **2021**, *85*, 106033. DOI
- Ren, Z.; Wang, K.; Sun, X. W.; Choy, W. C. H. Strategies toward efficient blue perovskite light-emitting diodes. *Adv. Funct. Mater.* **2021**, *31*, 2100516. DOI
- Bi, C.; Wang, S.; Li, Q.; Kershaw, S. V.; Tian, J.; Rogach, A. L. Thermally stable copper(II)-doped cesium lead halide perovskite quantum dots with strong blue emission. *J. Phys. Chem. Lett.* **2019**, *10*, 943-52. DOI
- Liu, R.; Xu, K. Blue perovskite light-emitting diodes (LEDs): a minireview. *Instrum. Sci. Technol.* **2020**, *48*, 616-36. DOI
- Shao, H.; Zhai, Y.; Wu, X.; et al. High brightness blue light-emitting diodes based on  $\text{CsPb}(\text{Cl}/\text{Br})_3$  perovskite QDs with phenethylammonium chloride passivation. *Nanoscale* **2020**, *12*, 11728-34. DOI
- Protesescu, L.; Yakunin, S.; Bodnarchuk, M. I.; et al. Nanocrystals of cesium lead halide perovskites ( $\text{CsPbX}_3$ , X = Cl, Br, and I): novel optoelectronic materials showing bright emission with wide color gamut. *Nano. Lett.* **2015**, *15*, 3692-6. DOI
- He, X.; Qiu, Y.; Yang, S. Fully-inorganic trihalide perovskite nanocrystals: a new research frontier of optoelectronic materials. *Adv. Mater.* **2017**, *29*. DOI
- Yang, X.; Ma, L.; Yu, M.; et al. Focus on perovskite emitters in blue light-emitting diodes. *Light. Sci. Appl.* **2023**, *12*, 177. DOI PubMed PMC
- Polavarapu, L.; Nickel, B.; Feldmann, J.; Urban, A. S. Advances in quantum-confined perovskite nanocrystals for optoelectronics. *Adv. Energy. Mater.* **2017**, *7*, 1700267. DOI
- Sichert, J. A.; Tong, Y.; Mutz, N.; et al. Quantum size effect in organometal halide perovskite nanoplatelets. *Nano. Lett.* **2015**, *15*, 6521-7. DOI
- Weidman, M. C.; Seitz, M.; Stranks, S. D.; Tisdale, W. A. Highly tunable colloidal perovskite nanoplatelets through variable cation, metal, and halide composition. *ACS. Nano.* **2016**, *10*, 7830-9. DOI PubMed
- Kumar, S.; Jagielski, J.; Yakunin, S.; et al. Efficient blue electroluminescence using quantum-confined two-dimensional perovskites. *ACS. Nano.* **2016**, *10*, 9720-9. DOI
- Kumar, S.; Jagielski, J.; Kallikounis, N.; et al. Ultrapure green light-emitting diodes using two-dimensional formamidinium perovskites: achieving recommendation 2020 Color coordinates. *Nano. Lett.* **2017**, *17*, 5277-84. DOI
- Wang, Y.; Wang, S.; Li, R.; et al. Quantum-confined perovskite nanocrystals enabled by negative catalyst strategy for efficient light-emitting diodes. *Small* **2024**, *20*, e2402825. DOI
- Chu, Z.; Zhao, Y.; Ma, F.; et al. Large cation ethylammonium incorporated perovskite for efficient and spectra stable blue light-emitting diodes. *Nat. Commun.* **2020**, *11*, 4165. DOI PubMed PMC
- Yuan, F.; Ran, C.; Zhang, L.; et al. A Cocktail of multiple cations in inorganic halide perovskite toward efficient and highly stable blue light-emitting diodes. *ACS. Energy. Lett.* **2020**, *5*, 1062-9. DOI
- Jiang, Y.; Qin, C.; Cui, M.; et al. Spectra stable blue perovskite light-emitting diodes. *Nat. Commun.* **2019**, *10*, 1868. DOI PubMed

## PMC

31. Liu, Y.; Cui, J.; Du, K.; et al. Efficient blue light-emitting diodes based on quantum-confined bromide perovskite nanostructures. *Nat. Photonics*. **2019**, *13*, 760-4. DOI
32. Zhang, M.; Zhang, J.; Zhao, G.; et al. Efficient blue CsPbBr<sub>3</sub> perovskite nanocrystals synthesis with the assistance of zwitterionic straight chain amino acids. *Colloids. Surf. A. Physicochem. Eng. Asp.* **2023**, *673*, 131793. DOI
33. Grandhi, G. K.; Likhiti, H. M.; Ong, S. P.; Im, W. B. Jahn-Teller distortion-driven robust blue-light-emitting perovskite nanoplatelets. *Appl. Mater. Today*. **2020**, *20*, 100668. DOI
34. Li, X.; Lou, B.; Chen, X.; et al. Deep-blue narrow-band emissive cesium europium bromide perovskite nanocrystals with record high emission efficiency for wide-color-gamut backlight displays. *Mater. Horiz.* **2024**, *11*, 1294-304. DOI
35. Xie, Y.; Peng, B.; Bravić, I.; et al. Highly Efficient blue-emitting CsPbBr<sub>3</sub> perovskite nanocrystals through neodymium doping. *Adv. Sci.* **2020**, *7*, 2001698. DOI
36. Guria, A. K.; Dutta, S. K.; Adhikari, S. D.; Pradhan, N. Doping Mn<sup>2+</sup> in lead halide perovskite nanocrystals: successes and challenges. *ACS. Energy. Lett.* **2017**, *2*, 1014-21. DOI
37. Feldmann, S.; Gangishetty, M. K.; Bravić, I.; et al. Charge carrier localization in doped perovskite nanocrystals enhances radiative recombination. *J. Am. Chem. Soc.* **2021**, *143*, 8647-53. DOI PubMed PMC
38. Liu, W.; Lin, Q.; Li, H.; et al. Mn<sup>2+</sup>-doped lead halide perovskite nanocrystals with dual-color emission controlled by halide content. *J. Am. Chem. Soc.* **2016**, *138*, 14954-61. DOI
39. Liu, Y.; Zhao, Y.; Zhu, Y.; Zhan, Y.; Matras-postolek, K.; Yang, P. Ion exchange derived CsPbBr<sub>3</sub>/Mn nanocrystals with stable and bright luminescence towards white light-emitting diodes. *Mater. Res. Bull.* **2022**, *153*, 111915. DOI
40. Hou, S.; Gangishetty, M. K.; Quan, Q.; Congreve, D. N. Efficient blue and white perovskite light-emitting diodes via manganese doping. *Joule* **2018**, *2*, 2421-33. DOI
41. Proppe, A. H.; Johnston, A.; Teale, S.; et al. Multication perovskite 2D/3D interfaces form via progressive dimensional reduction. *Nat. Commun.* **2021**, *12*, 3472. DOI PubMed PMC
42. Kim, Y. H.; Wolf, C.; Kim, Y. T.; et al. Highly efficient light-emitting diodes of colloidal metal-halide perovskite nanocrystals beyond quantum size. *ACS. Nano*. **2017**, *11*, 6586-93. DOI
43. Slimi, B.; Mollar, M.; Ben, A. I.; Kriaa, A.; Chtourou, R.; Mari, B. Synthesis and characterization of perovskite FAPbBr<sub>3-x</sub>I<sub>x</sub> thin films for solar cells. *Monatsh. Chem.* **2017**, *148*, 835-44. DOI
44. Yu, D.; Cai, B.; Cao, F.; et al. Cation exchange-induced dimensionality construction: from monolayered to multilayered 2D single crystal halide perovskites. *Adv. Mater. Interfaces*. **2017**, *4*, 1700441. DOI
45. Takeoka, Y.; Asai, K.; Rikukawa, M.; Sanui, K. Systematic studies on chain lengths, halide species, and well thicknesses for lead halide layered perovskite thin films. *Bull. Chem. Soc. Jpn.* **2006**, *79*, 1607-13. DOI
46. Zhang, D.; Eaton, S. W.; Yu, Y.; Dou, L.; Yang, P. Solution-phase synthesis of cesium lead halide perovskite nanowires. *J. Am. Chem. Soc.* **2015**, *137*, 9230-3. DOI PubMed
47. Pan, A.; He, B.; Fan, X.; et al. Insight into the ligand-mediated synthesis of colloidal CsPbBr<sub>3</sub> perovskite nanocrystals: the role of organic acid, base, and cesium precursors. *ACS. Nano*. **2016**, *10*, 7943-54. DOI
48. Sun, S.; Yuan, D.; Xu, Y.; Wang, A.; Deng, Z. Ligand-mediated synthesis of shape-controlled cesium lead halide perovskite nanocrystals via reprecipitation process at room temperature. *ACS. Nano*. **2016**, *10*, 3648-57. DOI